

Percolation of heterogeneous flows uncovers the bottlenecks of demand-serving networks

Homayoun Hamedmoghadam^a, Mahdi Jalili^b, Hai L. Vu^a, and Lewi Stone^{c,d}

^aInstitute of Transport Studies, Faculty of Engineering, Monash University, Melbourne, VIC 3800, Australia; ^bElectrical and Biomedical Engineering, School of Engineering, RMIT University, Melbourne, VIC 3000, Australia; ^cBiomathematics Unit, School of Zoology, Faculty of Life Sciences, Tel Aviv University, Tel Aviv 6997801, Israel;

^dMathematical Sciences, School of Science, RMIT University, Melbourne, VIC 3000, Australia

This manuscript was compiled on March 14, 2020

1 Whether it be the mobility demand of passengers in transportation
2 systems, or the energy demand of consumers in power grids, the
3 primary purpose of many physical infrastructures is to best serve
4 these different "flow demands" as they fluctuate unevenly across
5 complex networks. To assess the reliability of infrastructure net-
6 works, we propose a new theoretical percolation-based framework
7 that not only incorporates the network structure and link-level per-
8 turbations, but also caters for the heterogeneous flow demand dis-
9 tribution. The framework systematically takes into account that the
10 larger the flow demand between two nodes in the network, the more
11 crucial are their connecting paths, making the analysis more realistic
12 than current state-of-the-art approaches. The method also identifies
13 network "bottlenecks" that have guaranteed decisive effect by rupturing
14 network flows. Melbourne's bus and tram Public Transportation
15 (PT) network is digitally reconstructed based on >100-million smart-
16 card transaction records, and its functionality under actual pertur-
17 bations caused by road traffic congestion is analyzed by means of
18 the proposed framework. Ameliorating a small number of identified
19 bottlenecks is found to significantly improve network reliability and
20 reduce overall travel times, indicating the efficacy of the method. The
21 generality of the proposed method is also demonstrated on random
22 geometric graphs as a generic proxy for spatial networks. Our re-
23 sults suggest that embracing flow demand as a new dimension in
24 percolation analysis leads to a better understanding of complex in-
25 frastructure networks.

network analysis | percolation theory | bottleneck identification | flow demand

1 Recent theoretical advances in network science have con-
2 siderably contributed to our understanding of complex
3 systems, cutting across many disciplines from the social and
4 technological sciences, to the fields of ecology and biology (1–
5 12). In many modern studies, percolation theory (13, 14) has
6 been frequently employed to characterize structure, function-
7 ality and resilience of network systems. In this approach, link
8 failure is simulated by a percolation model which progressively
9 removes links from the network (15, 16). The impact is usually
10 measured via reduction in the size of the network's largest
11 connected component, or Giant Component (GC), as links
12 are gradually removed (17–19). Different strategies for simu-
13 lating link failures, e.g. random (error) or targeted (attack)
14 (20), make it possible to study a range of different topological
15 characteristics.

16 In real networks, links are consistently subject to various
17 forms of perturbations which often degrade their performance
18 in a continuous manner, rather than only causing complete
19 failure. To consider this, state-of-the-art approaches (21–23)
20 model the link-level dynamics on a network G by associating
21 each link e_{ij} (connecting node i to node j) with its own

"quality" attribute $q_{ij} \in (0, 1]$ at each time, which indicates
22 the temporal link performance relative to an observed or
23 predetermined maximum level of performance (24, 25). For
24 example, in a road traffic network, where the speed on each
25 road is changing temporally, link quality q_{ij} can be defined as
26 the ratio of instantaneous traffic speed to the limited maximal
27 speed on each link (23, 26), or in a communication network
28 link quality can be the relative instantaneous delivery rate
29 of information packets on a link (27). Typically, percolation
30 is simulated on such networks by increasing a threshold ρ
31 from 0 to 1 and simultaneously removing all links e_{ij} having
32 $q_{ij} \leq \rho$ from the initial network G to obtain G_ρ (28–30); see
33 the illustrated process on a small network in Fig. 1.
34

35 Of special interest is the critical threshold $\rho = \rho_c$ during
36 the percolation process at which the GC disintegrates into
37 components of smaller size. The percolation threshold ρ_c
38 can be an efficacious measure of global quality of network
39 structure, indicating that the network fails to provide global
40 connectivity with paths of links only having quality above
41 ρ_c (27, 31–33). While this generic critical phenomenon is of
42 vital importance for characterizing networks, we will show
43 that limiting attention exclusively to the GC and its sudden
44 disintegration reveals only a part of the full picture when
45 studying real-world problems.

46 The primary goal in many critical infrastructure networks
47 such as communication, power distribution, water supply, and
48 transportation systems, is to serve a certain demand for flow
49 movement; we refer to such systems as *demand-serving net-*

Significance Statement

A major characteristic of many infrastructural systems is the uneven demand for flow movement between different origin-destination points in the network. Unlike current state-of-the-art percolation analyses of perturbed networks, which assume this origin-to-destination flow demand is homogeneous, our proposed theoretical framework for the first time systematically takes into account the heterogeneity of flow demand. This is a significant addition to the modern network science where the heterogeneity of flow demand is often ignored in the analysis. The paper uncovers new network theoretic indices for assessing both network "reliability" and for finding "bottleneck" links, that will have important practical application in future studies of infrastructural network systems. New techniques for identifying network bottlenecks are shown to outperform the existing state-of-the-art methods.

Authors declare no competing interests.

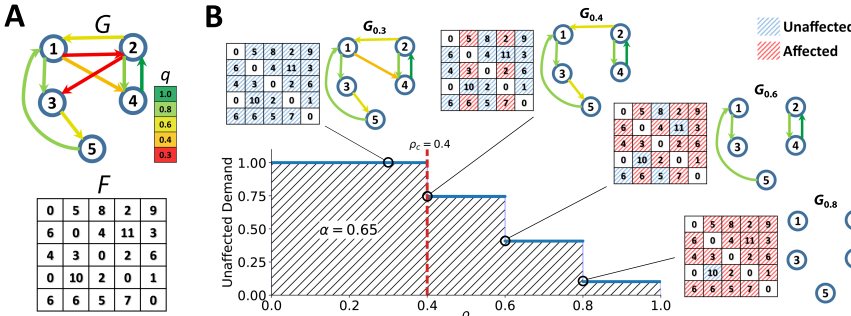


Fig. 1. Demand-serving reliability of an example network. (A) A demand-serving network of size $n = 5$ with color-coded link qualities. Matrix F shows the quantity of flow demand between all pairs of nodes which sums up to 100 units in total. (B) The percolation process is simulated by increasing a threshold ρ while removing links e_{ij} with $q_{ij} \leq \rho$. At multiple points in the process, the network is visualized with its corresponding affected (hatched red) and unaffected (hatched blue) flow demand. In this example, by definition, the system collapses at $\rho_c = 0.4$, when the 5-nodes strongly connected GC fragments into two strongly connected components of sizes 2 and 3, while Unaffected Demand (UD) is still at 75%. The network reliability α (Eq. 2) is calculated as the area under curve of UD between the limits of ρ (hatched in black).

works. In reality, the flow demand between Origin-Destination (O-D) node pairs is often distributed heterogeneously, and the larger the flow demand between two nodes, the more crucial are their connecting paths. In demand-serving networks, although the global connectivity is lost at percolation criticality, yet there might be a substantial flow demand inside isolated components in subcritical phase. For example, if the bulk of the flow demand is contained within small and medium-sized clusters (e.g. resulted from the disintegration of the GC), the network can remain highly functional even after the GC collapse (Fig. 1B). In other words, the global dynamics in demand-serving networks is not only controlled by structure and organization of link qualities, but also by the distribution of the flow demand over O-D pairs.

The goal of the present paper is to add further realism to percolation-based network analysis by inclusion of heterogeneous flow demand. Building upon state-of-the-art percolation-based network analyses (22, 23, 29), we introduce a calculus of network flows whereby known volumes of flux between each O-D pair become involved in the percolation process. This allows us to measure a network's ability to provide pathways of high quality (well-performing) links to satisfy the flow demand. We introduce a theoretical framework to quantify the extent of each link's contribution in rupturing paths on the network which we refer to as criticality score and use this to identify the network bottlenecks. Here, we first restrict our attention to a real transportation network as an exemplary instance of demand-serving networks, and then demonstrate the generality of our proposed framework. We show that the incorporation of the flow demand as an extra dimension to percolation-based network analysis can lead to different conclusions compared to those obtained solely from studying structural critical phenomena.

83 The case of a real demand-serving network

84 We demonstrate the application of the proposed framework, on
 85 the bus and tram (on-road) PT system in Melbourne, Australia,
 86 modeled using smart-card transaction data collected during
 87 September and October 2017. On-road PT systems are in
 88 constant conflict with road conditions, such as crowds, traffic,
 89 and signals, all negatively affecting the traveling flows by
 90 decelerating the PT vehicles. Separation of high demand O-D
 91 points by local pockets of congestion is an issue of considerable
 92 concern in transportation systems. The concept of O-D travel
 93 demand is fundamental to transportation theory (34), but only
 94 in this paper has it been made use of in studying passenger
 95 flows as a percolation-like process on dynamical transportation

networks.

Network $G(V, E, d, t)$ was generated for each day d and a moving 2-hour window centered at each time t of the day (see *Materials and Methods* and *SI Note 1*). Each node $i \in V$ corresponds to a cluster of closely situated bus and tram stops. A directed link $e_{ij} \in E$ connects node i to node j if there is at least one direct service between the two nodes. The flow demand matrix F was generated within the time window associated with each network, with each entry f_{ij} counting the number of passengers traveling from node i to node j via a single trip or multiple chained trips. Melbourne's on-road PT network is comprised of approximately 5,500 (2,800) nodes, 10,500 (4,500) links, and a flow demand derived from 470,000 (210,000) single-leg trips on average, during a normal weekday (weekend day).

In order to take into account the link-level perturbations caused by road conditions, similar to (22, 23) we assign a quality attribute to each link e_{ij} , calculated as:

$$q_{ij}(d, t) = \frac{\min_{t'}(\tau_{ij}(d, t'))}{\tau_{ij}(d, t)}. \quad [1]$$

Here, $\tau_{ij}(d, t)$ is the travel time on the link e_{ij} at time t of day d . The quality attribute $q_{ij}(d, t)$ indicates the link-level temporal performance of the network. At any point in time, a high-quality link has relatively low travel time (high velocity) compared to the rest of that day. In the following, for simplicity we refer to the network and its attributes without the day and time parameters. Figure 2A shows the spatial distribution of q_{ij} over the Melbourne's on-road PT network at 8:00 on 1 September 2017.

The percolation process illustrated in Fig. 2B for the Melbourne's PT network, indicates the loss of global connectivity at the percolation threshold of $\rho_c = 0.39$. However, as our analysis shows, at this point of criticality over 80% of trips can still be carried out between their O-D node pairs. This highlights a problem with interpreting ρ_c as a reliability index when the interest is on passenger flow demand. Note that this is not just a purely academic point. Stated in other words, previous methods (22, 23, 32), argue that if flows cannot reach location B from A without traversing low quality links, the transportation network has a problem. This is of course correct from a network connectivity perspective. On the other hand, a given passenger flow demand informs us about where the passenger flows begin and where they want to get to. Therefore, although location A is separated from location B with low quality links, it might not actually be important as much as the separation of other points, say, C from D where the flow

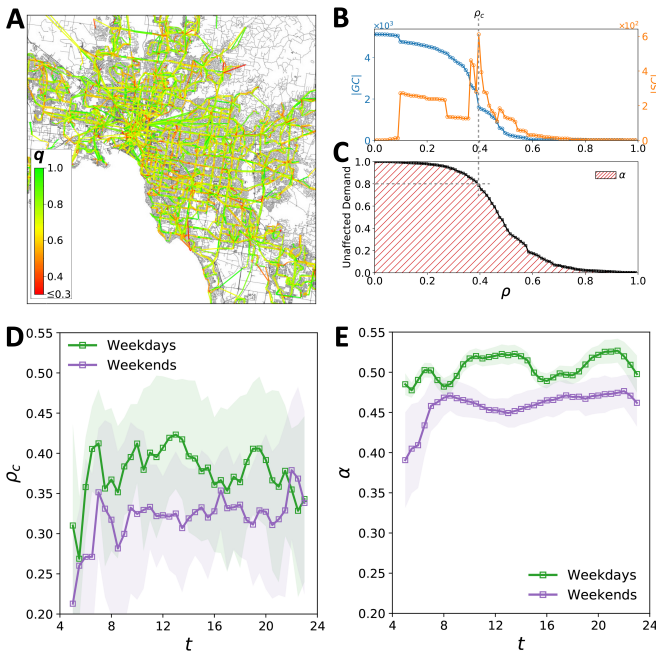


Fig. 2. Reliability of the Melbourne's bus and tram Public Transportation (PT) network. (A) The network representation of the PT system with colors indicating the link qualities q_{ij} for the period 7:00–9:00 (i.e. $t = 8$ and $\delta = 2$ h) on 1 September 2017. (B) Percolation process on the network illustrated in A, demonstrated by $|GC|$ and $|SC|$ as functions of threshold ρ ; the critical threshold $\rho = \rho_c$ is determined as the point of maximal $|SC|$ (vertical dashed gray line). (C) The same process as in B, demonstrated via UD_ρ , which shows the value of $\approx 80\%$ at percolation criticality (indicated by gray dashed lines). The proposed index α corresponds to the hatched area. Temporal evolution of (D) ρ_c and (E) α , during the day separately for weekdays (green) and weekends (purple). In D and E, curves show the mean over September and October 2017 and the shaded areas indicate the standard deviation of values around their mean. Note the much wider standard deviations for ρ_c in C.

links of the lowest quality (colored red) are removed, but this does not affect the flow demand between any pair of nodes, and thus $UD_{0.3} = 1$. When $\rho = 0.4$, however, removal of the link $1 \rightarrow 4$ impacts the UD as it prevents flows from reaching nodes 2 or 4 from either node 1, 3, or 5, by any pathway. The quantities of affected flows sum up to 25, thus the UD drops to $UD_{0.4} = 0.75$.

We now present our key index for assessing reliability of the demand-serving networks under link-level perturbations. We define the *demand-serving reliability* of the network, denoted by α , as the area under the curve of the UD_ρ over the domain of ρ (hatched area under curve in Fig. 1B), which can be formulated as:

$$\alpha = \int_0^1 UD_\rho d\rho = \int_0^1 \frac{\text{tr}(R_\rho F)}{\mathbf{1}_n^\top F \mathbf{1}_n} d\rho. \quad [2]$$

where $\text{tr}(\cdot)$ is the trace of the $n \times n$ square matrix, and $\mathbf{1}_n$ is a column vector of all n elements equal to one. In simple terms α gives an indication of average proportion of demand in the network that is unaffected as links are removed over the whole percolation process. As seen in Eq. 2 above, it is also possible to formulate UD_ρ , and as a result α , in simple mathematical terms making use of the network's so-called reachability matrix R and the flow demand matrix F (see *Materials and Methods*).

Let $|GC|$ be the size of the GC. In *Materials and Methods*, we show that when flow demand is distributed uniformly (i.e. f_{ij} equals a constant for any reachable pair of nodes i and j) then on any large-enough undirected network $|GC| \approx n\sqrt{UD}$ at any threshold during the percolation. Thus, only by assuming a uniform flow demand over the network, UD is able to replicate the percolation analysis based on monitoring the GC; this is also confirmed numerically later in the paper. Second, with heterogeneous flow demand, the last relation is no longer true and UD provides its unique description of the system dynamics with respect to the flow demand distribution. As a result, α can be a very useful indicator of network reliability as it captures the heterogeneity of flow demand through UD's behavior during the percolation.

Bottleneck identification

The framework suggests a new method for identifying network bottlenecks. Here, we introduce the link *criticality score* which quantifies the importance of each link quality for the demand-serving reliability of the network. The idea here is to examine all O-D pairs and seek out the links between them which are potentially the most responsible for controlling the quality of flow. The criticality score proposed here takes advantage of the work on the maximum capacity paths problem (35) to theoretically tie up the reachability of destinations from origins to percolation on the network. Suppose there is a set of different directed pathways Ψ_{OD} that connect node O to node D (see Fig. 3A). On each pathway $\psi \in \Psi_{OD}$, we search for the link with the minimum quality (Fig. 3B). Among those particular links, we choose the link with the maximum quality (Fig. 3C), denote it by e_{OD}^* , and refer to it as the *limiting link* associated with the ordered pair (O, D) . For simplicity, let us assume that each link quality value on the network is unique. Then, there will be only a single limiting link between any reachable pair of nodes. For a link e_{ij} , if $e_{OD}^* = e_{ij}$ for only

demand is far greater. The above issues motivate us to develop a new approach to capture the reliability of demand-serving networks, as an alternative to the critical percolation threshold, in order to enhance the understanding of such network systems.

Demand-serving network reliability α

Our approach is based on monitoring what we refer to as *Unaffected Demand* (UD), and requires keeping track of flows between all node pairs on the network during the percolation process. Network flow demand can be described by a square matrix $F = [f_{ij}]$ of order n equal to the network size, where each entry f_{ij} quantifies the flow from node i to node j (see Fig. 1A). At any threshold ρ , the flow demand f_{ij} is deemed to be "unaffected" if there is at least one directed path from i to j remaining on G_ρ . To assist in interpreting this, consider a link that is part of a path that begins from origin node i and reaches destination node j . If the link is removed, and there is still at least one other directed pathway from i to j , the flow demand remains unaffected by the link removal. We define UD_ρ as the fraction of total flow demand that is not affected by removal of links performing with quality below the threshold ρ ; see *Materials and Methods* for detailed formulation.

It is instructive to examine how UD_ρ varies with increasing ρ on the example network shown in Fig. 1A, where the total flow demand is 100 by some arbitrary unit of measurement and $UD_0 = 100/100$ initially. When $\rho = 0.3$ (Fig. 1B), two

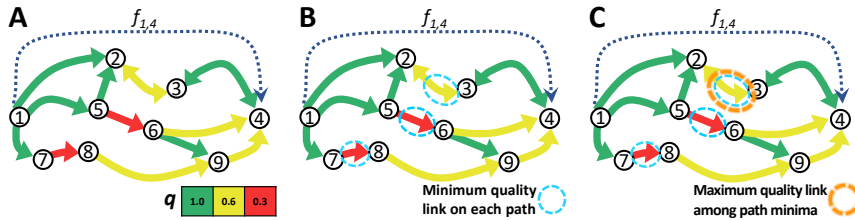


Fig. 3. Finding the limiting link between an origin-destination node pair. (A) As an example, we look for the limiting link associated with O-D node pair (1, 4) with flow demand $f_{1,4}$. (B) The available paths from node 1 to node 4 (and their associated minimum-quality links) are $1 \rightarrow 2 \rightarrow 3 \rightarrow 4$ ($e_{2,3}$), $1 \rightarrow 5 \rightarrow 2 \rightarrow 3 \rightarrow 4$ ($e_{2,3}$), $1 \rightarrow 5 \rightarrow 6 \rightarrow 4$ ($e_{5,6}$), $1 \rightarrow 5 \rightarrow 6 \rightarrow 9 \rightarrow 4$ ($e_{5,6}$), $1 \rightarrow 7 \rightarrow 8 \rightarrow 9 \rightarrow 4$ ($e_{7,8}$). (C) Among the minimum-quality links of these paths, $e_{2,3}$ has the maximum quality. Just below the threshold $\rho = 0.6$, still two paths connect nodes 1 to 4, but then with $e_{2,3}$ removed, node 4 becomes unreachable from node 1. The limiting link for node pair (1, 4) is $e_{2,3}$ as increase in $q_{2,3}$ will keep the pair connected for longer during the percolation. The ratio of $f_{1,4}$ to the total demand is added to $s_{2,3}$ to reflect the importance of $e_{2,3}$ for demanded flow from node 1 to 4.

a single pair (O, D), then the link criticality score s_{ij} will be the fraction of the total demand that flows from O to D , i.e.

$$s_{ij} = \frac{f_{OD}}{\mathbf{1}_n^T F \mathbf{1}_n}. \quad [3]$$

The index relies on the feature that during the percolation, as soon as the threshold ρ reaches the value q_{ij} , removal of the limiting link e_{ij} results in complete rupture of all pathways from O to D . If the link e_{ij} is the limiting link between several node pairs (see Fig. S4), Eq. 3 extends to:

$$s_{ij} = \sum_{O, D \in V, e_{OD}^* = e_{ij}} \frac{f_{OD}}{\mathbf{1}_n^T F \mathbf{1}_n}. \quad [4]$$

We have identified an important relationship that connects the link quality (q_{ij}), the link criticality score (s_{ij}), and the network reliability (α), namely:

$$\sum_{e_{ij} \in E} s_{ij} \cdot q_{ij} = \alpha, \quad [5]$$

as proven in *Materials and Methods*. It can be rigorously shown that for any link e_{ij} , increasing q_{ij} within a non-empty range will increase the network reliability α , with the magnitude of increase being proportional to s_{ij} (see SI Note 4). (This is a nontrivial problem since alteration of the quality of any link in the network can change the criticality score of multiple links.) As such, links with larger criticality scores have greater influence on network reliability α . Therefore, after ranking the links according to their criticality scores, a desired number of the top critical links can be identified as network bottlenecks. For our experiments on Melbourne's PT network, we chose the top 2% in the ranking of critical links as the network bottlenecks.

Reliability of Melbourne's on-road PT network

We return now to use the above tools to study the Melbourne PT network. Figure 2B illustrates the percolation process on Melbourne's bus and tram (on-road) PT network (at 8:00 on 1 September 2017) through $|GC|$ and the size of the Second-largest Component ($|SC|$) as functions of ρ . In practice, the percolation threshold is determined as the threshold $\rho = \rho_c$ at which $|SC|$ is maximal (36). In Fig. 2B the point of maximal $|SC|$ captures the GC collapse, however, this was not always the case at other times and dates. The GC fragmentation during the percolation process was often blurred out rather than demonstrating a drastic change in $|GC|$, or in other cases,

appeared as multiple peaks in $|SC|$ which makes it difficult (if not impossible) to identify the critical threshold (Fig. S2); Ref. (37) reported similar phenomena in road network of multiple cities. The index α evaluates the network according to the whole percolation process and does not depend on existence of a clear phase transition, making the above issue irrelevant.

Figure 2C demonstrates the percolation process shown in Fig. 2B, but this time with UD as a function of ρ . As pointed out before, the figure reveals that at criticality ($\rho_c = 0.39$), 80% of trips can nevertheless be carried out between their O-D points ($UD_{0.39} = 0.8$), which empirically demonstrates how characterizing a network based on ρ_c alone can be misleading when flow demand distribution is heterogeneous. The reliability indicator α leverages the concept of UD to account for the fact that pathways between different node pairs are not equally important to the reliability of the network. In effect, during the link removal process UD does not necessarily decline with the same rate as pairwise connectivity (see SI Note 2 and Fig. S3). In Melbourne's PT network, the number of connected node pairs decrease faster than UD, meaning that demand is higher within clusters of high-quality links in the network.

We examined both ρ_c and α on Melbourne's PT network over the main functioning hours of the system during two months of September and October 2017, separately for weekdays and weekends. Temporally, ρ_c had unusually large fluctuations over the day, and there appeared to be no repeating pattern on a day to day comparison (Fig. 2D). For further details regarding these intense fluctuations compare Figs. S4A and S4C. In contrast, the proposed reliability measure α followed a clear daily pattern (Fig. 2E) with variations that have relatively small standard deviation. The approximately 10% drops in α at 8:00 and 16:00-18:00 on weekdays are associated with morning and evening peak commuting periods, when high rates of congestion and large numbers of commuters predictably increase the conflict between PT system and road conditions. Consistent daily evolution of α with circadian rhythm of urban human mobility, and its low variability over different days suggest its success in unravelling the repeating daily pattern in complex interactions between major constituents of the system, namely, supply network structure, link-level perturbations, and passenger flow demand (also see SI Note 3). The results also suggest that Melbourne's PT network is relatively stable over a day, despite multiple periods of intense traffic, which is partially due to more available PT services during the rush hours which increase the number of links and thus network density.

Figure 2E shows that α varied temporally in two different ranges during weekdays and weekends, implying that the network functions in two separate modes. Despite larger flow demand and more extensive congestions, α was larger for weekdays compared to weekends. This is explained by the observed phenomenon in Fig. S3, which shows that a higher volume of flow has to traverse lower quality links during weekends compared to weekdays, which expectedly lowered the demand-serving reliability of the network.

Bottlenecks of Melbourne's PT network

In Melbourne's on-road PT network, link criticality scores vary over time. Therefore, we calculate the mean criticality score of each link over the course of the available data, and identify the network bottlenecks as links with the largest mean criticality scores, separately for weekdays and weekends. The identified bottlenecks are shown to be robust and occur as highly critical links on most days (Fig. S8).

The spatial distribution of the link criticality scores is portrayed in Fig. 4A. In the actual network, flow demand is significantly high to or from urban hotspot locations (38). Pockets of traffic congestions and crowds, which decrease the quality of PT network links, usually form around these hotspots. As a result, during both weekdays and weekends (Fig. S9A), links with large criticality scores were found to be generally in alignment with the urban morphology, as they were situated in urban hotspots and the areas surrounding them. Specifically, the biggest urban shopping center is surrounded by links with high criticality scores, and the top bottlenecks were mostly distributed around the single most significant hotspot of Melbourne which is the Central Business District (CBD). Also, universities are good examples of urban hotspots which are only fully active on weekdays. Among the top network bottlenecks, we observed links to and from major universities (Fig. 4B), emerging only on weekdays (see Fig. S9B). Given that the proposed method does not incorporate any geo-spatial information from the network, the surprising alignment between the locations pinned by identified bottlenecks and the hotspots of Melbourne's urban area, suggests that the method is capturing actuality.

We also observed that four out of the top ten "pain points" on Melbourne's road network (39) reported in the media, are in very close proximity to links among our identified top bottlenecks at morning rush hour. Since almost half of these ten points do not have bus or tram services in conflict with the road conditions, the results suggest that our methodology does indeed work well.

The impact of bottleneck amelioration

It is interesting to compare the effectiveness of our proposed Criticality Score-based (CS) bottleneck identification scheme, to other well-established bottleneck identification schemes (see SI Note 5). In particular, we compare against the widely-used edge betweenness centrality measure (40), here referred to as EB bottlenecks. The bottlenecks found by this scheme are the links bridging between the locally well-connected communities of the network. Alternatively, bottlenecks can be identified among the links removed at percolation criticality as used in (22), which we refer to as PC bottlenecks. These bottlenecks, termed "red bonds" in percolation theory (41), glue the GC together by connecting the communities of higher quality links.

To make comparisons between these approaches, we ameliorated specific bottlenecks and monitored the response of the network in terms of changes to the demand-serving reliability α . In practice, the most obvious proposal for enhancing the reliability of an on-road PT network is to reduce the conflict of PT vehicles with road conditions at network bottlenecks, which can be done for example by giving signal priority to PT vehicles or allocating segregated (exclusive) PT lanes. Here again, the bottlenecks are taken to be the top 2% most critical links in the network over time, according to each approach. Let B denote the set of bottlenecks identified by one of the schemes. We ameliorated the bottlenecks by synthetically increasing the qualities of bottleneck links $e_{ij} \in B$, to unity ($q_{ij} = 1$). Figures 4C compares the impact of amelioration on bottlenecks for the three different approaches, as a function of time during weekdays (see Fig. S11 for the results on weekends). Complete amelioration of the CS bottlenecks resulted in more than 22% (25%) improvement in α , on average during weekdays (weekends). Amelioration of EB and PC bottlenecks increased α over any day by approximately 8% and 6% on average, respectively.

The investigation was extended by verifying the impact of bottleneck amelioration on reducing the delay in passenger travel times, as a more intuitive efficiency measure for transportation networks. In order to calculate the delay caused by perturbations, we first generated an unperturbed copy of the network at each time of a day by changing the actual travel time on each link to the minimum travel time observed on that link during the day. We assumed that each trip took place on the directed path with minimum sum of the link travel times, between origin and destination nodes. Then, for any particular network, delay was calculated as the absolute difference between the total travel time on the actual and the unperturbed copy of the network. Delay indicates the extent of the impeding effect of perturbations on passenger trips.

Separately for weekdays and weekends, we simulated the amelioration of the top CS, EB, and PC bottlenecks (the top 2% most critical links based on each scheme). Ameliorating the CS bottlenecks decreased the delay per passenger trip from 5.3 min (5.7 min) to 3.8 min (4.2 min) during weekdays (weekends). Figure 4D shows the temporal delay per passenger on the actual and ameliorated temporal network during the first five weekdays in September 2017; Fig. S12 extends Fig. 4D over the months of available data. Amelioration of EB (PC) bottlenecks had almost half (less than half) the reduction effect of CS bottlenecks on delay per trip. The time saved by amelioration of CS bottlenecks compared to that of EB (PC) bottlenecks is almost twofold (more than twofold). The result of ameliorating the top CS bottlenecks was close to 2,000 hours of passenger travel time saved only during morning rush hours (7:00-9:00) on the network, and approximately 11,000 hours of passenger travel time over a normal weekday.

Generality of the proposed framework

In order to emphasize the generality of the proposed framework, we used a Random Geometric Graph model (RGG) as a generic proxy of spatial networks and showed the ability of the framework to reflect the true global flow properties of the network. Here, undirected RGG networks were generated by first distributing 10^4 nodes uniformly at random on the plane $[0, 100]^2$, and then connecting any pair of nodes with

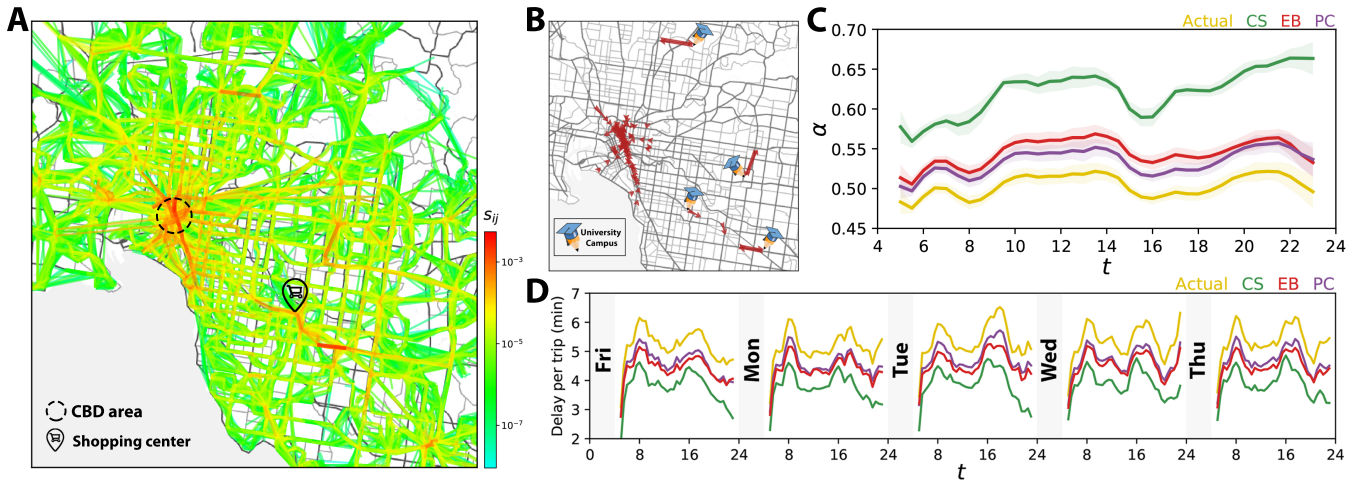


Fig. 4. Bottleneck identification and amelioration on a real-world network. (A) Spatial distribution of the link criticality scores s_{ij} over Melbourne's Public Transportation (PT) network during weekdays. The Central Business District (CBD) and the biggest shopping center in Melbourne are pinned on the map. (B) Top 100 weekday bottlenecks of Melbourne's PT network, identified based on link criticality scores. Major university campuses outside Melbourne's CBD area are pinned on the map. C and D compare the impact of ameliorating perturbations on bottlenecks identified based on Criticality Score (CS), Edge Betweenness centrality (EB), and Percolation Criticality (PC); the number of identified bottlenecks by each approach is equal to 2% of the number of links that appear on the network over time. (C) Daily evolution of α calculated for the actual (yellow) and ameliorated networks associated with different bottleneck identification approaches. Results show the average (solid line) and standard deviation (shaded area) over the weekdays of September and October 2017. (D) Delay per trip in minutes caused by road perturbations, on the actual and networks in which bottlenecks are ameliorated.

Euclidean distance below $r = 1.5$. Each link quality was drawn uniformly at random from $(0, 1]$, making percolation a random link removal process which depends only on the network topology. RGGs are built of clusters with high intra-connectivity glued together by bridging links (Fig. 5A). This structure demonstrates a clear phase transition during the percolation process, when enough inter-cluster links are removed to make a significant part of the network isolated from the rest (Fig. 5B).

Over each RGG instance, we distributed a fixed total flow demand volume, according to three different scenarios, namely, uniform, short-range, and long-range. In the uniform demand scenario, the total flow demand volume was divided equally among all reachable (O, D) node pairs; i.e. all entries of F , corresponding to a reachable node pair, are equal to a constant. Let d_{ij} be the Euclidean distance between nodes i and j , and d_{max} the distance between the most distant node pair in the network. Then, to generate the short-range (long-range) flow demand scenarios, we repeatedly picked a node pair (O, D) uniformly at random and then with probability $0.2e^{-0.2d_{OD}}$ ($0.2e^{-0.2(d_{max}-d_{OD})}$) added one unit to the flow demand between that O-D pair f_{OD} , until the fixed total flow demand volume was completely allocated over the network.

We simulated the percolation for each one of the above flow demand distributions, on 100 realizations of RGG structure. During the percolation, we monitored the GC and SC, which are independent from the demand distribution, and also UD for the three demand distribution scenarios (Fig. 5B & C). Remarkably, in Fig. 5C for the case of uniform flow, the percolation diagram as a function of ρ is the same for UD as it is for the square of $|GC|$ (normalized with the network size). Thus, simulation results confirm the previously discussed theoretical relationship $UD_\rho \approx (|GC_\rho|/n)^2$ between evolution of the GC and UD when demand is uniformly distributed over the network (Fig. 5C). This shows that by assuming a uniform flow demand over the network, our method can provide an analogous analysis to that of monitoring the GC.

Furthermore, UD shows logical sensitivity to non-uniformity of flow demand distributions on network reliability. Long-range flows are more likely to break in the event of GC collapse, which UD reflected with a faster decrease as a function of increasing ρ (Fig. 5C). This resulted in a lower demand-serving reliability ($\alpha = 0.43$) compared to the case of uniform demand ($\alpha = 0.50$). In contrast, highly-connected local communities in RGG preserve the short-range flows during the percolation. Hence the network becomes more reliable which was reflected by a higher α ($= 0.58$).

Here, we verify the sensibility of the bottlenecks identified based on link criticality scores for RGG networks. We use the link overlap $\eta \in [0, 1]$ to determine whether a link belongs to a community (high overlap) or acts as an inter-community bridge (low overlap); overlap of a link e_{ij} is defined as $\eta_{ij} = \frac{|\Gamma(i) \cap \Gamma(j)|}{|\Gamma(i) \cup \Gamma(j)| - 2}$ where $\Gamma(i)$ is the neighborhood set of node i . In Fig. 5A links are color-coded according to their overlap index. The criticality score of intra-community (high overlap) links was found to be higher for short-range flow demand scenario compared to the long-range scenario (Fig. 5D). This is consistent with the fact that short-range flows are more likely to have their origin and destination within a community, which makes the flow-carrying role of intra-community links more critical. Inter-community (low overlap) links have a bigger role in bridging between the remote points of the network, thus, with higher flow exchange between the distant nodes these links become more critical for reliability of the network. As expected, criticality score of inter-community links were higher in long-range flow scenario compared to short-range flow scenario.

Conclusion

In this paper, we proposed the demand-serving network reliability index α , which quantifies the ability of networks to provide pathways of high-quality links to satisfy the flow demand between O-D nodes. By constructing the theoretical relationship

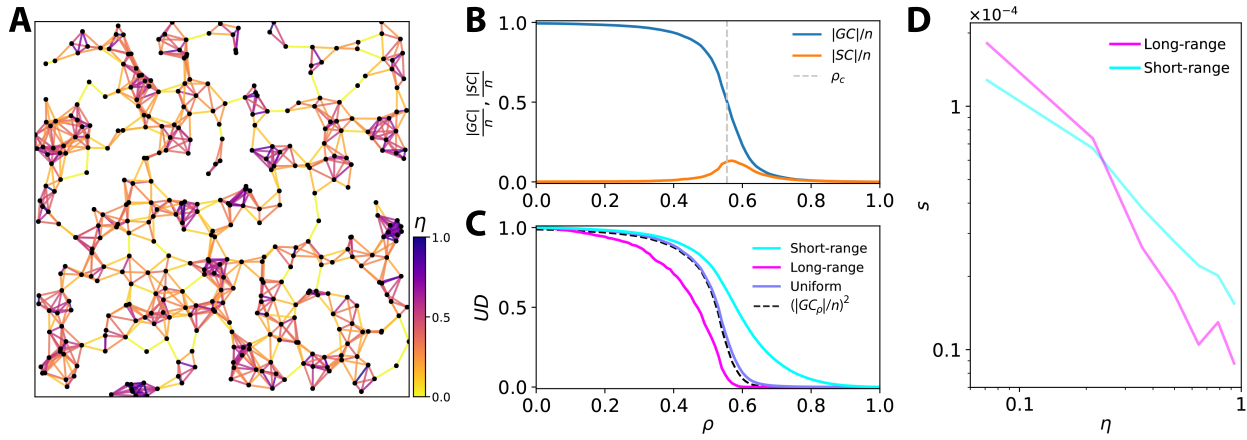


Fig. 5. Capturing true properties of the demand-serving networks. (A) A sample RGG with $n = 400$ spread over the plane $[0, 20]^2$, with each link colored based on its overlap index η . (B) Normalized $|GC|$ and $|SC|$ during the percolation process averaged over 100 realizations of RGG structure with $n = 10^4$ nodes and random link qualities. (C) Unaffected Demand (UD) versus ρ for different flow demand scenarios on the RGG structure, averaged over 100 realizations. As predicted, evolution of size of the GC during the percolation process is approximately equal to $n \sqrt{UD_\rho}$ when the flow demand is uniform; compare the blue and dashed black curves. (D) Criticality score s versus overlap η of links, compared for short-range and long-range flow demand scenarios.

between the link qualities and percolation dynamics on the network, we introduced a bottleneck identification approach. Our proposed framework is generally applicable to demand-serving networks including most physical infrastructures such as transportation, communication, power distribution, and water supply networks, where the inherent demand for flow movement between different nodes makes the connectivity between some nodes more important than others.

With link quality attribute describing the link-level dynamics in a network, percolation analysis (21–23, 29, 32) can be the lead for understanding the global quality of network structure. However, when dealing with demand-serving networks, the proposed index α leverages the introduced "unaffected demand" concept to account for the heterogeneity of node-to-node flow volumes, and thus unveils the otherwise obscure global flow quality on the network. Similarly, the bottleneck identification method introduced here, is a more comprehensive approach for such networks and proved more effective than other schemes reported in the literature in terms of both improving the network reliability and reducing the delay caused by link-level perturbations in the presented real-world application.

With ever-increasing availability of data, this study can be a starting point for diverse experiments on real-world networks with known flow demand. Our aim is to also open new avenues for more sophisticated theoretical work on the implications of flow demand on global dynamics of demand-serving networks, which should aid us to obtain a more profound understanding of these complex systems.

Materials and Methods

Smart-card data. The data used in the real-world case study, are the smart-card transaction records, collected by the Automated Fare Collection (AFC) system for PT in Melbourne, Australia. Passengers are supposed to perform a scan-on transaction at the start and a scan-off at the end of their trip. Every smart-card transaction record contains multiple attributes, namely, anonymized card identifier, PT mode (bus, tram, or train), vehicle identifier (unique number for each bus or tram vehicle), stop identifier, timestamp, and transaction type (scan-on/off). We used an average of over

2,120,000 and 912,000 daily transactions associated with all PT modes on weekdays and weekends, respectively, collected during 61 days of September and October 2017. After applying a cleaning process, we used the data to generate the temporal network of on-road PT supply and its corresponding passenger travel flow demand (see SI Note 1 for details).

Network and flow demand matrix construction. To generate the network (details provided in SI Note 1) representation of the on-road PT system in Melbourne at time t on a particular day, the smart-card data was limited to the time window $[t - \delta/2, t + \delta/2]$, where the time window length δ , was set to 2 hours for experiments presented in the main article. First, we clustered the closely located PT stops and mapped each cluster to a node. Using information of smart-card transactions we derived the trajectory of every vehicle on the network, and if there was at least one vehicle traveling from one of the stops associated with node i to a stop associated with node j without stopping, we added a direct link e_{ij} starting at node i and pointing at node j . For each link e_{ij} the average travel time τ_{ij} over the time window was also calculated based on the information from the tracked vehicles. For network of time t , flow demand matrix F measures the demand volumes by the number journeys between nodes, within the time window used for construction of the network. A journey is a chain of one or more trip legs with transfers (but no activities) in between them; see SI Note 1 on how single trip legs are chained to obtain journeys. Throughout this manuscript, unless otherwise stated, a "trip" refers to a journey.

Unaffected Demand (UD). To formulate the UD calculation, we use the so-called reachability matrix $R = [r_{ij}]$ (the transitive closure of the network adjacency matrix) which is a square matrix of order n . Each entry r_{ij} is equal to 1 if there is at least one directed path from node i to node j on the network, and $r_{ij} = 0$ otherwise. Let R_ρ be the reachability matrix of network G_ρ . At any threshold ρ , the flow demand f_{ij} is deemed to be unaffected if there is at least one directed path from i to j remaining on G_ρ , i.e. $r_{ij}^\rho = 1$. So, UD_ρ will be the sum of $r_{ij}^\rho \cdot f_{ij}$ for all (i, j) pairs of nodes, normalized by the total flow demand:

$$UD_\rho = \frac{\mathbf{1}_n^T (R_\rho \circ F) \mathbf{1}_n}{\mathbf{1}_n^T F \mathbf{1}_n} = \frac{\text{tr}(R_\rho F)}{\mathbf{1}_n^T F \mathbf{1}_n}, \quad [6]$$

where " \circ " is the entry-wise product of matrices, $\text{tr}(\cdot)$ is the trace of the $n \times n$ square matrix, and $\mathbf{1}_n$ is a column vector of all n elements equal to one.

Relation between the evolution of UD and GC during the percolation. Let $|GC_\rho|$ be the size of the GC as a function of ρ , then $|GC_\rho|/n$ is called the incipient order parameter which is sometimes used to

- describe the connectivity of a fragmented network. If we assume a uniform flow demand distribution then on any undirected network, UD_ρ equals the proportion of connected node pairs at ρ , which approaches $(|GC_\rho|/n)^2$ as $n \rightarrow \infty$ (42). So, for large enough networks, monitoring the GC during the percolation is spacial case of monitoring UD when flow demand is uniform. Therefore, we can accurately predict the evolution of $|GC|$ during the percolation by assuming a uniform flow demand over the network and using $|GC_\rho| \approx n\sqrt{UD_\rho}$. This is confirmed numerically in Fig. 5.
- Link criticality score.** Suppose that there exists a non-empty set of different directed pathways Ψ_{OD} that route between an origin node O and a reachable destination node D . During the percolation process on the network (whereby ρ is increased from zero to unity), each pathway $\psi \in \Psi_{OD}$ breaks up when the threshold ρ reaches to the minimum link-quality on that path. The limiting link associated with flow from O to D (e_{OD}^*), when removed during the percolation process at $\rho = q_{OD}^*$, breaks the last path(s) connecting O to D and affects the flow between them (f_{OD}). Using the definition of link criticality score in Eq. 4, we can expand the left-hand-side of Eq. 5 as:
- $$\sum_{e_{ij} \in E} s_{ij} \cdot q_{ij} = \sum_{e_{ij} \in E} \sum_{\substack{O, D \in V, \\ e_{OD}^* = e_{ij}}} \frac{f_{OD}}{\mathbf{1}_n^T F \mathbf{1}_n} \cdot q_{ij} = \frac{1}{\mathbf{1}_n^T F \mathbf{1}_n} \sum_{O, D \in V} \sum_{\substack{e_{ij} \in E \\ e_{OD}^* = e_{ij}}} f_{OD} \cdot q_{ij}, \quad [7]$$
- and for any pair $O, D \in V$ with non-zero f_{OD} there exist a single limiting link $e_{OD}^* \in E$ with quality q_{OD}^* , so
- $$= \frac{1}{\mathbf{1}_n^T F \mathbf{1}_n} \sum_{O, D \in V} f_{OD} \cdot q_{OD}^*. \quad [8]$$
- By definition, during the percolation process, each entry in the reachability matrix R_ρ switches from 1 to 0 as soon as the last path(s) between its corresponding O-D nodes break. So, we can write:
- $$r_{OD}^\rho = \begin{cases} 1, & \rho < q_{OD}^*, \\ 0, & \rho \geq q_{OD}^*, \end{cases} \quad [9]$$
- where r_{OD}^ρ is the (O, D) entry of the reachability matrix R_ρ associated with the network G_ρ . Note that the integral of r_{OD}^ρ with respect to ρ between the limits $\rho = 0$ and $\rho = 1$ is equal to q_{OD}^* . So, from Eq. 8 and Eq. 9 we can write:
- $$\sum_{e_{ij} \in E} s_{ij} \cdot q_{ij} = \frac{1}{\mathbf{1}_n^T F \mathbf{1}_n} \sum_{O, D \in V} f_{OD} \cdot \int_0^1 r_{OD}^\rho d\rho, \quad [10]$$
- where the right-hand-side can be simplified with matrix operations to obtain Eq. 2 which is the definition of the reliability index α , so we can conclude that Eq. 5 holds. In SI Note 4, the definition of the criticality score and the proof of Eq. 5 are generalized further, requiring no assumption on the link quality values.
- ACKNOWLEDGMENTS.** We thank Prof. Shlomo Havlin for his extremely helpful discussions of the ideas presented in this paper and for his suggestions. Also, we thank Dr. Meead Saberi for the fruitful discussions, and Nora Estgfaeller for providing valuable feedback throughout this study. M.J. and L.S. are supported by Australian Research Council (ARC) through project No. DP170102303. M.J. is also supported by ARC through project No. DP200101119. H.V. is supported by ARC through project Nos. DP180102551 and DP190102134.
1. SV Buldyrev, R Parshani, G Paul, HE Stanley, S Havlin, Catastrophic cascade of failures in interdependent networks. *Nature* **464**, 1025–1028 (2010).
2. M Jalili, M Perc, Information cascades in complex networks. *J. Complex Networks* **5**, 665–693 (2017).
3. D Duan, et al., Universal behavior of cascading failures in interdependent networks. *Proc. Natl. Acad. Sci.* **116**, 22452–22457 (2019).
4. O Askarishani, et al., Structural balance emerges and explains performance in risky decision-making. *Nat. Commun.* **10**, 1–10 (2019).
5. A Barja, et al., Assessing the risk of default propagation in interconnected sectoral financial networks. *EPJ Data Sci.* **8**, 32 (2019).
6. M De Domenico, A Baronchelli, The fragility of decentralised trustless socio-technical systems. *EPJ Data Sci.* **8**, 2 (2019).
7. J Gao, B Barzel, AL Barabási, Universal resilience patterns in complex networks. *Nature* **530**, 307–312 (2016).
8. L Stone, The google matrix controls the stability of structured ecological and biological networks. *Nat. Commun.* **7**, 12857 (2016).
9. SM Hill, et al., Inferring causal molecular networks: empirical assessment through a community-based effort. *Nat. Methods* **13**, 310–318 (2016).
10. L Stone, The feasibility and stability of large complex biological networks: a random matrix approach. *Sci. Reports* **8**, 1–12 (2018).
11. M Santolini, AL Barabási, Predicting perturbation patterns from the topology of biological networks. *Proc. Natl. Acad. Sci.* **115**, E6375–E6383 (2018).
12. L Stone, D Simberloff, Y Artzy-Randrup, Network motifs and their origins. *PLoS Comput. Biol.* **15** (2019).
13. HE Stanley, *Introduction to phase transitions and critical phenomena*. (Oxford: Clarendon Press), (1971).
14. A Bunde, S Havlin, *Fractals and disordered systems*. (Springer Science & Business Media), (2012).
15. AA Ganin, et al., Resilience and efficiency in transportation networks. *Sci. advances* **3**, e1701079 (2017).
16. V Latora, M Marchiori, Vulnerability and protection of infrastructure networks. *Phys. Rev. E* **71**, 015103 (2005).
17. M De Domenico, A Solé-Ribalta, S Gómez, A Arenas, Navigability of interconnected networks under random failures. *Proc. Natl. Acad. Sci.* **111**, 8351–8356 (2014).
18. B Mirzsoleiman, M Babaei, M Jalili, M Safari, Cascaded failures in weighted networks. *Phys. Rev. E* **84**, 046114 (2011).
19. M Jalili, Error and attack tolerance of small-worldness in complex networks. *J. Informetrics* **5**, 422–430 (2011).
20. R Albert, H Jeong, AL Barabási, Error and attack tolerance of complex networks. *Nature* **406**, 378–382 (2000).
21. A Halu, A Scala, A Khiyami, MC González, Data-driven modeling of solar-powered urban microgrids. *Sci. Adv.* **2**, e1500700 (2016).
22. D Li, et al., Percolation transition in dynamical traffic network with evolving critical bottlenecks. *Proc. Natl. Acad. Sci.* **112**, 669–672 (2015).
23. G Zeng, et al., Switch between critical percolation modes in city traffic dynamics. *Proc. Natl. Acad. Sci.* **116**, 23–28 (2019).
24. L Zhang, G Zeng, S Guo, D Li, Z Gao, Comparison of traffic reliability index with real traffic data. *EPJ Data Sci.* **6**, 19 (2017).
25. F Wang, D Li, X Xu, R Wu, S Havlin, Percolation properties in a traffic model. *Europhys. Lett.* **112**, 38001 (2015).
26. M Saberi, et al., A simple contagion process describes spreading of traffic jams in urban networks. *Nat. Commun.* (in press).
27. P Echenique, J Gómez-Gardenes, Y Moreno, Dynamics of jamming transitions in complex networks. *Europhys. Lett.* **71**, 325 (2005).
28. LK Gallos, HA Makse, M Sigman, A small world of weak ties provides optimal global integration of self-similar modules in functional brain networks. *Proc. Natl. Acad. Sci.* **109**, 2825–2830 (2012).
29. YN Kenett, et al., Flexibility of thought in high creative individuals represented by percolation analysis. *Proc. Natl. Acad. Sci.* **115**, 867–872 (2018).
30. J Borge-Holthoefer, Y Moreno, A Arenas, Topological versus dynamical robustness in a lexical network. *Int. J. Bifurc. Chaos* **22**, 1250157 (2012).
31. SD Reis, et al., Avoiding catastrophic failure in correlated networks of networks. *Nat. Phys.* **10**, 762–767 (2014).
32. D Li, Q Zhang, E Zio, S Havlin, R Kang, Network reliability analysis based on percolation theory. *Reliab. Eng. & Syst. Saf.* **142**, 556–562 (2015).
33. R Cohen, S Havlin, *Complex networks: structure, robustness and function*. (Cambridge University Press), (2010).
34. N Oppenheim, *Urban travel demand modeling: from individual choices to general equilibrium*. (John Wiley and Sons), (1995).
35. M Pollack, Letter to the editor—the maximum capacity through a network. *Oper. Res.* **8**, 733–736 (1960).
36. DS Callaway, ME Newman, SH Strogatz, DJ Watts, Network robustness and fragility: Percolation on random graphs. *Phys. Rev. Lett.* **85**, 5468 (2000).
37. LE Olmos, S Çolak, S Shafei, M Saberi, MC González, Macroscopic dynamics and the collapse of urban traffic. *Proc. Natl. Acad. Sci.* **115**, 12654–12661 (2018).
38. H Hamedmoghadam, M Ramezani, M Saberi, Revealing latent characteristics of mobility networks with coarse-graining. *Sci. Reports* **9**, 1–10 (2019).
39. 2018 redspot survey. (<https://www.redspotsurvey.com.au>) (2018) [Accessed 14/02/2020].
40. M Girvan, ME Newman, Community structure in social and biological networks. *Proc. Natl. Acad. Sci.* **99**, 7821–7826 (2002).
41. D Ben-Avraham, S Havlin, *Diffusion and reactions in fractals and disordered systems*. (Cambridge University Press), (2000).
42. Y Chen, et al., Percolation theory applied to measures of fragmentation in social networks. *Phys. Rev. E* **75**, 046107 (2007).